

A Parametric Family of Polynomial Wavelets for Signal and Image Processing

Mariantonia Cotronei^{a,*}, Woula Themistoclakis^b, Marc Van Barel^c

^a*DIIES, Università Mediterranea di Reggio Calabria, Via Zehender Loc. Feo di Vito, Reggio Calabria, 89122, Italy*

^b*C.N.R. National Research Council of Italy, IAC Institute for Applied Computation “Mauro Picone”, Via P. Castellino 111, Naples, 80131, Italy*

^c*Department of Computer Science, KU Leuven, Celestijnenlaan 200A, Heverlee, B-3001, Belgium*

Abstract

This paper investigates the potential applications of a parametric family of polynomial wavelets that has been recently introduced starting from de la Vallée Poussin (VP) interpolation at Chebyshev nodes. Unlike classical wavelets, which are constructed on the real line, these VP wavelets are defined on a bounded interval, offering the advantage of handling boundaries naturally while maintaining computational efficiency. In addition, the structure of these wavelets enables the use of fast algorithms for decomposition and reconstruction. Furthermore, the flexibility offered by a free parameter allows a better control of localized singularities, such as edges in images. On the basis of previous theoretical foundations, we show the effectiveness of the VP wavelets for basic signal denoising and image compression, emphasizing their potential for more advanced signal and image processing tasks.

Keywords: Wavelets; Multiresolution analysis; De la Vallée Poussin interpolation; Sparse representations; Denoising; Compression

1. Introduction

Wavelet transforms are widely recognized as powerful tools in various applications, particularly in signal and image processing, being able to effectively extract frequency content from data and represent them using a reduced set of information.

Our goal is to contribute to the extensive research developed over the past decades by implementing and testing a special class of wavelet transforms based on a non-standard multiresolution analysis in which the resolution level is tripled instead

*Corresponding author

Email addresses: mariantonia.cotronei@unirc.it (Mariantonia Cotronei), woula.themistoclakis@cnr.it (Woula Themistoclakis), marc.vanbareel@kuleuven.be (Marc Van Barel)

of doubled at each step. Specifically, we consider a parametric family of wavelets recently introduced in [12], constructed without any dilation and translation but using de la Vallée Poussin (briefly VP) interpolation at Chebyshev nodes [13, 14, 15]. These VP wavelets are interpolating, non-orthogonal, polynomials. They are defined on $[-1, 1]$, to which any other compact interval can be mapped, and can be easily generalized to higher dimensions via tensor products. Thus, unlike classical wavelets, data on finite domains can be naturally processed by VP wavelets without the need for additional modifications. Furthermore, even with the uniform norm, they possess good approximation properties, which can be further controlled through a free parameter.

In addition, the structure of the VP wavelets allows for the implementation of fast algorithms for data decomposition and reconstruction, ensuring computational efficiency.

In this paper, after presenting the main properties of the new wavelet basis, we describe the implementation of the corresponding transform and inverse transform, providing details relevant to their correct application in signal processing.

We then focus on two classical applications: signal denoising and image compression. In such contexts, our goal is not to develop new algorithms, but to demonstrate the potential performance of the proposed basis, particularly in comparison with standard wavelet filters.

The paper is organized as follows: Section 2 introduces the univariate VP scaling and wavelet functions, detailing their construction and key properties. Section 3 presents the decomposition and reconstruction algorithms, along with details of a correct application in signal processing. Sections 5 and 6 discuss the application of VP wavelets to signal denoising and image compression, respectively, providing experimental results and comparisons with traditional wavelet methods. Finally, conclusions are drawn, highlighting potential future directions.

2. Univariate VP scaling and wavelet functions

For any $n \in \mathbb{N}$, we denote the zeros of the Chebyshev polynomial $T_n(x) = \cos(n \arccos x)$ by

$$x_k^n := \cos \frac{(2k-1)\pi}{2n}, \quad k = 1, \dots, n.$$

They are also zeros of $T_{3n}(x)$ and specifically we have

$$x_k^n = x_{3k-1}^{3n}, \quad k = 1, \dots, n.$$

The remaining zeros of T_{3n} , which are not zeros of T_n , are denoted by y_k^n with $k = 1, \dots, 2n$. More precisely, we set

$$y_{2k-1}^n := x_{3k-2}^{3n} \quad \text{and} \quad y_{2k}^n := x_{3k}^{3n}, \quad k = 1, \dots, n.$$

The two sets of Chebyshev zeros

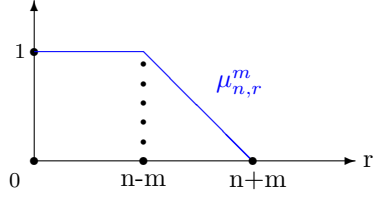
$$X_n := \{x_k^n : k = 1, \dots, n\} \quad \text{and} \quad Y_n = \{y_k^n : k = 1, \dots, 2n\}$$

constitute the interpolation nodes of the scaling and wavelet functions, which we are going to define below.

To this aim, we make use of the following polynomial kernel [12]

$$\phi_n^m(x, y) = \frac{2}{n} \sum_{r=0}^{n+m-1} {}' \mu_{n,r}^m T_r(x) T_r(y), \quad n, m \in \mathbb{N}, \quad 0 < m < n, \quad (1)$$

where the notation \sum' means that the first addendum of the summation is halved, and the coefficients $\mu_{n,r}^m$ are defined as follows

$$\mu_{n,r}^m := \begin{cases} 1 & \text{if } 0 \leq r \leq n-m, \\ \frac{m+n-r}{2m} & \text{if } n-m < r < n+m, \end{cases}$$


Equivalently, ϕ_n^m can be written in the following trigonometric form [10]

$$\phi_n^m(\cos t, \cos s) = \frac{1}{4nm} \left(\frac{\sin[n(t-s)] \sin[m(t-s)]}{\sin^2[(t-s)/2]} + \frac{\sin[n(t+s)] \sin[m(t+s)]}{\sin^2[(t+s)/2]} \right).$$

Under the previous notation, for all $x \in [-1, 1]$, each resolution level $n \in \mathbb{N}$ and any integer parameter $0 < m < n$, the *VP scaling functions* are defined as follows [12]

$$\phi_{n,k}^m(x) = \phi_n^m(x_k^n, x), \quad k = 1, \dots, n, \quad (2)$$

while the *VP wavelets* are

$$\psi_{n,k}^m(x) = \phi_{3n}^m(y_k^n, x) - \sum_{h=1}^n \phi_{n,h}^m(y_k^n) \phi_{3n}^m(x_h^n, x), \quad k = 1, \dots, 2n. \quad (3)$$

Let us summarize the main properties of these polynomials valid for any pair of integers $0 < m < n$ [12].

1. *Interpolation.* Using the Kronecker delta, we have

$$\phi_{n,k}^m(x_h^n) = \delta_{h,k}, \quad h, k = 1, \dots, n, \quad (4)$$

$$\psi_{n,k}^m(y_h^n) = \delta_{h,k}, \quad h, k = 1, \dots, 2n. \quad (5)$$

2. *Moments.* Setting $dw(x) = \frac{dx}{\sqrt{1-x^2}}$, for all $r = 0, 1, \dots, n-m$, we have

$$\int_{-1}^1 x^r \phi_{n,k}^m(x) dw(x) = (x_k^n)^r, \quad k = 1, \dots, n, \quad (6)$$

$$\int_{-1}^1 x^r \psi_{n,k}^m(x) dw(x) = 0, \quad k = 1, \dots, 2n. \quad (7)$$

3. *Stability.* Setting, for any function f ,

$$\|f\|_p = \begin{cases} \left(\int_{-1}^1 |f(x)|^p w(x) dx \right)^{\frac{1}{p}} & 1 \leq p < \infty, \\ \sup_{|x| \leq 1} |f(x)| & p = \infty, \end{cases}$$

and, for any vector $\vec{v}_N = (v_1, \dots, v_N) \in \mathbb{R}^N$,

$$\|\vec{v}_N\|_{\ell^p} = \begin{cases} \left(\frac{\pi}{N} \sum_{k=1}^N |v_k|^p \right)^{\frac{1}{p}} & 1 \leq p < \infty, \\ \max_{1 \leq k \leq N} |v_k| & p = \infty, \end{cases}$$

we have that for any $1 \leq p \leq \infty$ and all vectors $\vec{a}_n = (a_1, \dots, a_n) \in \mathbb{R}^n$, and $\vec{b}_{2n} = (b_1, \dots, b_{2n}) \in \mathbb{R}^{2n}$, the following inequalities

$$\mathcal{C}_1 \|\vec{a}_n\|_{\ell^p} \leq \left\| \sum_{k=1}^n a_k \phi_{n,k}^m \right\|_p \leq \mathcal{C}_2 \left(1 + \log \frac{n}{m} \right) \|\vec{a}_n\|_{\ell^p}, \quad (8)$$

$$\mathcal{C}_3 \|\vec{b}_{2n}\|_{\ell^p} \leq \left\| \sum_{k=1}^{2n} b_k \psi_{n,k}^m \right\|_p \leq \mathcal{C}_4 \left(1 + \log^2 \frac{n}{m} \right) \|\vec{b}_{2n}\|_{\ell^p}, \quad (9)$$

hold, where $\mathcal{C}_i > 0$, $i = 1, \dots, 4$, are constants independent of \vec{a}_n , \vec{b}_{2n} , n and m .

4. *Convergence.* For any fixed $\theta \in]0, 1[$, if we take $m = \lfloor \theta n \rfloor$ and a sufficiently large resolution level $n \in \mathbb{N}$, then any continuous function f on $[-1, 1]$ can be uniformly approximated with the desired precision by the VP interpolation polynomial [14]

$$V_n^m f(x) := \sum_{k=1}^n f(x_k^n) \phi_{n,k}^m(x), \quad x \in [-1, 1], \quad (10)$$

namely, we have

$$\lim_{\substack{n \rightarrow \infty \\ m = \lfloor \theta n \rfloor}} \|f - V_n^m f\|_{\infty} = 0, \quad \forall f \in C^0[-1, 1], \quad \forall \theta \in]0, 1[. \quad (11)$$

Moreover, we have the same convergence order of the error of best polynomial approximation $E_n(f) := \inf_{\deg(P) \leq n} \|f - P\|_{\infty}$, which depends on the smoothness degree of f [8]. In particular, if f is Hölder continuous with exponent $0 < \alpha \leq 1$ then we have

$$\|f - V_n^m f\|_{\infty} = \mathcal{O}(n^{-\alpha}) \quad (12)$$

Furthermore, if f is continuously differentiable up to order $2s$, for some $s \in \mathbb{N}$, then we have [11, Thm. 5.3]

$$\|f^{(r)} - (V_n^m f)^{(r)}\|_{\infty} = \mathcal{O}(n^{-2s+r}), \quad r = 0, 1, \dots, s \quad (13)$$

where $f^{(r)}$ denotes the r -th derivative of f , and $f^{(0)} := f$.

3. Decomposition and reconstruction algorithms

The above defined VP scaling and wavelet functions generate a multiresolution analysis, whose approximation and detail spaces, at a given resolution level $n \in \mathbb{N}$ and arbitrarily fixed parameter $m < n$, are defined as follows

$$\mathcal{V}_n^m = \text{span} \{ \phi_{n,k}^m, k = 1, \dots, n \}, \quad \dim \mathcal{V}_n^m = n, \quad (14)$$

$$\mathcal{W}_n^m = \text{span} \{ \psi_{n,k}^m, k = 1, \dots, 2n \}, \quad \dim \mathcal{W}_n^m = 2n. \quad (15)$$

They satisfy [12]

$$\mathcal{V}_{3n}^m = \mathcal{V}_n^m \oplus \mathcal{W}_n^m \quad \text{and} \quad \mathcal{V}_n^m \perp \mathcal{W}_n^m, \quad \forall n > m \in \mathbb{N}, \quad (16)$$

where orthogonality is understood w.r.t. the scalar product

$$\langle f, g \rangle := \int_{-1}^1 f(x)g(x)dw(x), \quad dw(x) = \frac{dx}{\sqrt{1-x^2}}.$$

Consequently, any function $f_{3n} \in \mathcal{V}_{3n}^m$ can be uniquely decomposed as

$$f_{3n} = f_n + g_{2n}, \quad \text{with} \quad f_n \in \mathcal{V}_n^m \quad \text{and} \quad g_{2n} \in \mathcal{W}_n^m. \quad (17)$$

Using the interpolating bases (14)–(15), these functions are uniquely determined by their basis coefficients, i.e., we have

$$f_n(x) = \sum_{k=1}^n a_{n,k} \Phi_{n,k}^m(x), \quad a_{n,k} = f_n(x_k^n), \quad \forall f_n \in \mathcal{V}_n^m \quad (18)$$

$$g_{2n}(x) = \sum_{k=1}^{2n} b_{n,k} \psi_{n,k}^m(x), \quad b_{n,k} = g_{2n}(y_k^n), \quad \forall g_{2n} \in \mathcal{W}_n^m. \quad (19)$$

Fast decomposition and reconstruction algorithms can be given in order to compute the basis coefficients of f_n and g_{2n} from the basis coefficients of f_{3n} , and viceversa [12, Thm. 5.2].

Setting

$$p_r(x) = \sqrt{\frac{2}{\pi}} \frac{T_{r-1}(x)}{\sqrt{1+\delta_{r,1}}}, \quad r = 1, 2, \dots$$

and

$$q_r(x) = \begin{cases} p_r(x) & r = 1, \dots, n-m+1 \\ \frac{m+(n-r+1)}{2m} p_r(x) - \frac{m-(n-r+1)}{2m} p_{2n-r+2}(x) & r = n-m+2, \dots, n \end{cases}$$

these algorithms are based on the following discrete transforms

- $\vec{u} = \mathcal{T}_1(\vec{v})$ that transforms $\vec{v} = (v_1, \dots, v_n)$ in $\vec{u} \in \mathbb{R}^n$ with entries

$$u_r = \sum_{s=1}^n v_s p_r(x_s^n), \quad r = 1, \dots, n$$

- $\vec{u} = \mathcal{T}_2(\vec{v})$ that transforms $\vec{v} = (v_1, \dots, v_n)$ in $\vec{u} \in \mathbb{R}^n$ with entries

$$u_s = \sum_{r=1}^n v_r p_r(x_s^n), \quad r = 1, \dots, n$$

- $\vec{u} = \mathcal{T}_3(\vec{v})$ that transforms $\vec{v} = (v_1, \dots, v_{2n})$ in $\vec{u} \in \mathbb{R}^n$ with entries

$$u_r = \sum_{s=1}^{2n} v_s q_r(y_s^n), \quad r = 1, \dots, n$$

- $\vec{u} = \mathcal{T}_4(\vec{v})$ that transforms $\vec{v} = (v_1, \dots, v_n)$ in $\vec{u} \in \mathbb{R}^{2n}$ with entries

$$u_s = \sum_{r=1}^n v_r q_r(y_s^n), \quad s = 1, \dots, 2n$$

By using the previous transforms the decomposition and reconstruction algorithms can be schematized as follows

Algorithm 1 Decomposition

Input: \vec{a}_{3n} basis coeff. of $f_{3n} = f_n + g_{2n}$

Output: \vec{a}_n and \vec{b}_n basis coeff. of f_n and g_{2n}

```

1: for  $k = 1 : n$  do
2:    $v_k = a_{3n, 3k-1}$ 
3:    $u_{2k-1} = a_{3n, 3k-2}$ 
4:    $u_{2k} = a_{3n, 3k}$ 
5: end for
6:  $\vec{x} = \frac{\pi}{3n} \mathcal{T}_1(\vec{v})$ 
7:  $\vec{y} = \frac{\pi}{3n} \mathcal{T}_3(\vec{u})$ 
8: for  $k = 1 : n - m + 1$  do
9:    $v_k = x_k + y_k$ 
10: end for
11: for  $k = n - m + 2 : n$  do
12:    $v_k = \frac{2m^2(x_k + y_k)}{m^2 + (n - k + 1)^2}$ 
13: end for
14:  $\vec{a}_n = \mathcal{T}_2(\vec{v})$ 
15:  $\vec{b}_n = \mathcal{T}_4(\vec{v})$ 

```

Algorithm 2 Reconstruction

Input: \vec{a}_n and \vec{b}_n basis coeff. of f_n and g_{2n}

Output: \vec{a}_{3n} basis coeff. of $f_{3n} = f_n + g_{2n}$

```

1:  $\vec{x} = \frac{\pi}{n} \mathcal{T}_1(\vec{a}_n)$ 
2:  $\vec{y} = \frac{\pi}{3n} \mathcal{T}_3(\vec{b}_n)$ 
3:  $\vec{u} = \vec{a}_n - \mathcal{T}_2(\vec{y})$ 
4:  $\vec{v} = \vec{b}_n + \mathcal{T}_4(\vec{x})$ 
5: for  $k = 1 : n$  do
6:    $a_{3n, 3k-1} = u_k$ 
7:    $a_{3n, 3k-2} = v_{2k-1}$ 
8:    $a_{3n, 3k} = v_{2k}$ 
9: end for

```

As observed in [12], each transform \mathcal{T}_i can be efficiently computed using $\mathcal{O}(n \log n)$ flops by means of the well-known *discrete cosine transform* (DCT) and its inverse

(IDCT), in Matlab known as DCT of type 2 and 3, respectively. They transform any $\vec{v} = (v_1, \dots, v_N) \in \mathbb{R}^N$ in $\vec{u} \in \mathbb{R}^N$ defined as follows

- $\vec{u} = DCT(\vec{v})$ has entries $u_r = \sqrt{\frac{2}{N}} \frac{1}{\sqrt{1 + \delta_{r,1}}} \sum_{s=1}^N v_s T_{r-1}(x_s^N), \quad r = 1, \dots, N$
- $\vec{u} = IDCT(\vec{v})$ has entries $u_s = \sqrt{\frac{2}{N}} \sum_{r=1}^N \frac{v_r}{\sqrt{1 + \delta_{r,1}}} T_{r-1}(x_s^N), \quad s = 1, \dots, N.$

Using these transforms, we have

$$\mathcal{T}_1(\vec{v}) = \sqrt{\frac{n}{\pi}} DCT(\vec{v}) \quad \text{and} \quad \mathcal{T}_2(\vec{v}) = \sqrt{\frac{n}{\pi}} IDCT(\vec{v}), \quad \forall \vec{v} \in \mathbb{R}^n.$$

Moreover, the transforms \mathcal{T}_3 and \mathcal{T}_4 can be computed using the following algorithms.

Algorithm 3 Compute $\vec{u} = \mathcal{T}_3(\vec{v})$

Input: $\vec{v} = (v_1, \dots, v_{2n})$

Output: $\vec{u} = (u_1, \dots, u_n)$

```

1: for  $k = 1 : n$  do
2:    $w_{3k-2} = v_{2k-1}$ 
3:    $w_{3k-1} = 0$ 
4:    $w_{3k} = v_{2k}$ 
5: end for
6:  $\vec{x} = \sqrt{\frac{3n}{\pi}} DCT(\vec{w})$ 
7: for  $k = 1 : n - m + 1$  do
8:    $u_k = x_k$ 
9: end for
10: for  $k = n - m + 2 : n$  do
11:    $u_k = \frac{m+(n-k+1)}{2m} x_k - \frac{m-(n-k+1)}{2m} x_{2n-k+2}$ 
12: end for
```

Algorithm 4 Compute $\vec{u} = \mathcal{T}_4(\vec{v})$

Input: $\vec{v} = (v_1, \dots, v_n)$

Output: $\vec{u} = (u_1, \dots, u_{2n})$

```

1: for  $k = 1 : n - m + 1$  do
2:    $w_k = v_k$ 
3: end for
4: for  $k = n - m + 2 : n$  do
5:    $w_k = \frac{m+(n-k+1)}{2m} v_k$ 
6:    $w_{2n-k+2} = -\frac{m-(n-k+1)}{2m} v_k$ 
7: end for
8: for  $k = n + m + 4 : 3n$  do
9:    $w_k = 0$ 
10: end for
11:  $\vec{x} = \sqrt{\frac{3n}{\pi}} IDCT(\vec{w})$ 
12: for  $k = 1 : n$  do
13:    $u_{2k-1} = x_{3k-2}$ 
14:    $u_{2k} = x_{3k}$ 
15: end for
```

3.1. Application to signal processing

The application of VP bases to signal processing requires some considerations. First of all, let us discuss about the mathematical model to adopt. As is well known, a digital signal is mathematically represented by a vector, say $\vec{v} = (v_1, \dots, v_N)$, of a certain length N . Its elements are typically considered as the values assumed by a certain function on N equidistant nodes of an interval, which we can assume to be $[-1, 1]$ without violating generality. In our model, we consider equidistant nodes not on the segment $[-1, 1]$ but on the semicircle, i.e.

$$t_k = \frac{(2k-1)\pi}{2N}, \quad k = 1, \dots, N,$$

and we assume that behind the signal there exists a function f , representing it in the continuum, such that

$$v_k = f(\cos t_k), \quad k = 1, \dots, N.$$

Thus, using these samples we can approximate f , and hence the signal, by its projection onto the space \mathcal{V}_N , i.e., by the VP interpolation polynomial

$$V_N^m f(x) = \sum_{k=1}^N v_k \phi_{N,k}^m(x), \quad m = \lfloor \theta N \rfloor, \quad \theta \in]0, 1[, \quad x \in [-1, 1],$$

and we can handle the signal with the usual wavelet techniques by applying the previous decomposition and reconstruction algorithms.

We now have to face two problems: the first concerns N , which according to our scheme should be a multiple of three, the second concerns the conservation of the signal energy.

To address the first issue, we extend the vector \vec{v} by replicating its last element until its length becomes divisible by three, after which we apply the decomposition algorithm. During reconstruction, the vector of scaling coefficients is then truncated to restore the original length.

Regarding the second problem, since the VP scaling and wavelet functions are interpolating and not orthogonal, the Parseval identity is not applicable, and appropriate correction factors must be considered both in decomposition and reconstruction for energy conservation. Traditionally, in case of non-orthogonal wavelets, the scaling and wavelet coefficients are usually multiplied by $\sqrt{2}$ after the decomposition, and divided by $\sqrt{2}$ before the reconstruction. In our case, we multiply/divide the scaling coefficients by $\sqrt{3}$ and the wavelet coefficients by $\sqrt{3/2}$. To justify this, we observe that $f_{3n} = f_n + g_{2n}$ and $f_n \perp g_{2n}$ imply

$$\|f_{3n}\|_2^2 = \|f_n\|_2^2 + \|g_{2n}\|_2^2. \quad (20)$$

On the other hand, by (18)-(19), and (8)-(9) we get

$$\|f_{3n}\|_2^2 \sim \left(\frac{\pi}{3n} \sum_{k=1}^{3n} a_{3n,k}^2 \right), \quad \|f_n\|_2^2 \sim \left(\frac{\pi}{n} \sum_{k=1}^n a_{n,k}^2 \right), \quad \|g_{2n}\|_2^2 \sim \left(\frac{\pi}{2n} \sum_{k=1}^{2n} b_{n,k}^2 \right),$$

where by $A \sim B$ we mean that there exist absolute constants $\mathcal{C}_1, \mathcal{C}_2 > 0$ (independent of the resolution level and the coefficients) such that $\mathcal{C}_1 A \leq B \leq \mathcal{C}_2 A$.

Consequently, from (20) we deduce

$$\frac{\pi}{3n} \sum_{k=1}^{3n} a_{3n,k}^2 \sim \frac{\pi}{n} \sum_{k=1}^n a_{n,k}^2 + \frac{\pi}{2n} \sum_{k=1}^{2n} b_{n,k}^2$$

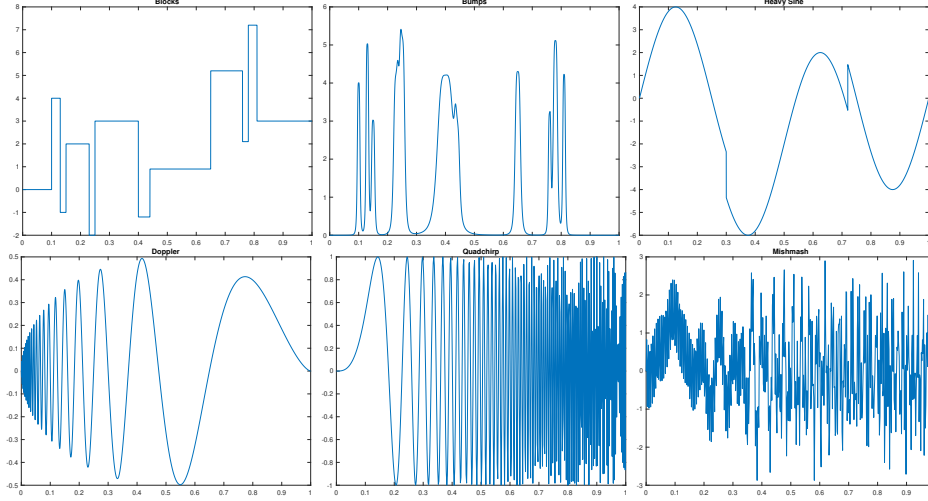


Figure 1: Six wavelet test functions: Blocks, Bumps, Heavy Sine, Doppler, Quadchirp, Mishmash.

that yields

$$\sum_{k=1}^{3n} a_{3n,k}^2 \sim \sum_{k=1}^n (\sqrt{3}a_{n,k})^2 + \sum_{k=1}^{2n} \left(\sqrt{\frac{3}{2}} b_{n,k} \right)^2. \quad (21)$$

With the described algorithms and all the above observations in mind, we now proceed to test the VP basis through experiments on two typical data processing tasks: signal denoising and image compression. In the first case, we use univariate VP wavelets, in the second case we deal with bidimensional VP wavelets. The bivariate extension of the VP wavelets is obtained through a standard tensor product approach of the univariate scaling and wavelet functions. According to the previous semicircular sampling model, it is assumed that the equidistant pixel grid of the image is mapped to the grid of Chebyshev nodes. Following the standard procedure, the algorithms described above are applied iteratively to the columns and rows of the image data.

4. Signal denoising

Wavelet transform-based methods have proven to be highly effective in signal denoising tasks. The goal is to recover a signal $s = (s_k : k = 1, \dots, n)$ from noisy observations $y = (y_k : k = 1, \dots, n)$:

$$y_k = s_k + \eta_k, \quad k = 1, \dots, n,$$

where $\eta_k \sim \mathcal{N}(0, \sigma^2)$ are independent and identically distributed (i.i.d.) Gaussian random variables with mean 0 and variance σ^2 .

Several different algorithms for wavelet-based signal denoising have been proposed in the literature, starting with the pioneering works by Donoho and Johnstone [6, 7].

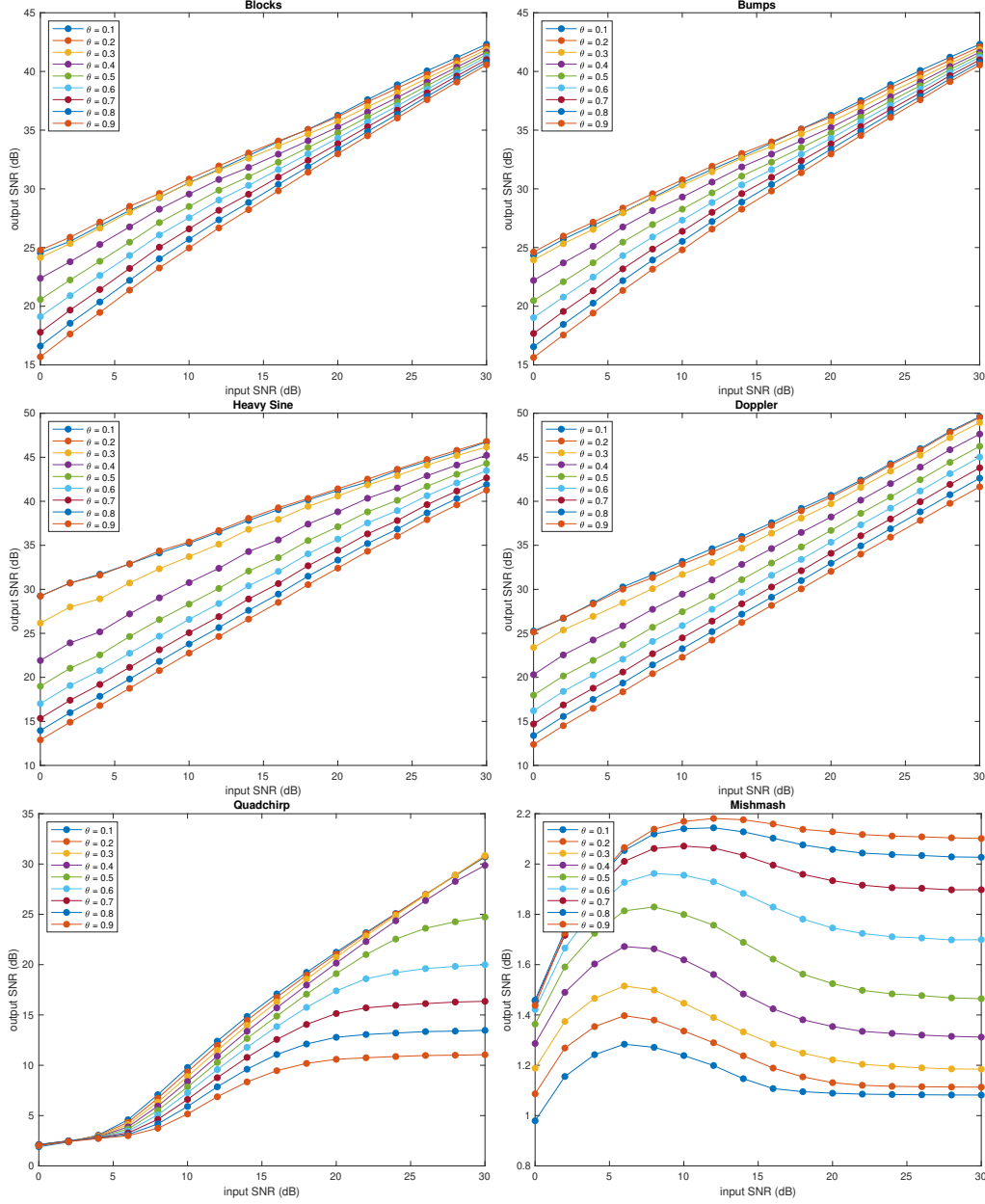


Figure 2: The results for different values of $\theta = 0.1, 0.2, \dots, 0.9$ for the six wavelet test functions: Blocks, Bumps, Heavy Sine, Doppler, Quadchirp, Mishmash.

Each method applies a different thresholding strategy to separate the signal from the noise.

In this context, we aimed at testing such methods when used in conjunction with VP wavelets, assessing their performance in comparison with standard wavelet filters. In our preliminary experiments, it was found that the Bayesian method [5] with soft thresholding produced the best results.

To refine the normalization factors as proposed at the end of the previous section (cf.

21) we took 1000 Gaussian random signals with mean 0 and variance 1. These signals were decomposed and the standard deviation for each of the detail components and for the approximation component was measured. For each of the detail components and the approximation component the average of these standard deviations was taken as the normalisation factor for the corresponding component. The magnitude of these normalization factors turned out to be around 1.

To determine how the parameter θ influences the reconstruction results, we applied the Bayes method to the six wavelet test functions of the wavelet toolbox of Matlab¹: Blocks, Bumps, Heavy Sine, Doppler, Quadchirp and Mishmash, plotted in Fig. 1.

For each of these test functions we executed the Bayes method with soft thresholding for parameter values θ ranging from 0.1 to 0.9. The length of the input signals was 2^{17} . For each value of θ 10 samples of the input signal were considered and the average was taken.

In Fig. 2, the result is plotted for the six test functions. This figure shows the signal-to-noise ratio (SNR) of the input signal with respect to the SNR of the output signal. We recall that the SNR of the two signals s_1 and s_2 is defined as

$$\text{SNR}(s_1, s_2) = 10 \log_{10} \left(\frac{\sigma_{signal}^2}{\sigma_{noise}^2} \right)$$

with σ_{signal}^2 the variance of the signal s_1 and σ_{noise}^2 the variance of the noise signal, i.e., the difference between the signals s_1 and s_2 . The input SNR is defined as the SNR of the original signal and the noisy signal while the output SNR is defined as the SNR of the original signal and the denoised signal.

From the plots it is clear that the value $\theta = 0.1$ is best or near-best for the 6 test functions. Hence, in the sequel, we fixed the value of θ to be equal to 0.1.

In the next experiment, we compared our denoising method with the one of Matlab “wdenoise” (of the wavelet toolbox) for all choices of the wavelets that are available using this denoising function: bior1.1, bior1.3, bior1.5, bior2.2, bior2.4, bior2.6, coif1, coif2, coif3, coif4, coif5, db2, db3, db4, db5, db6, db7, db8, db9, db10, db11, rbio1.3, rbio1.5, rbio2.2, rbio2.4, rbio2.6, rbio2.8, sym2, sym3, sym4, sym5, sym6, sym7. Applying “wdenoise”, we used the default denoising method which is “Bayes” and soft thresholding. Also here we took the average of 10 samples. Figure 3 shows the results for the 6 wavelet test functions.

For “Blocks”, our method is not performing well compared to the others. In this case the best three wavelets are bior1.1, bior1.5 and bior1.3. For “Bumps” our method is the best one for all values of the input SNR. For “Heavy Sine” our method is the best for small values of the input SNR. For “Doppler” also our method is one of the best for small values of the input SNR. For “Quadchirp” our method is the best for almost all values of the input SNR. For small values of the input SNR, bior2.6 is slightly better. For “Mishmash” our method performs well with respect to the

¹We used Matlab version R2024B. Matlab is a registered trademark of the MathWorks.

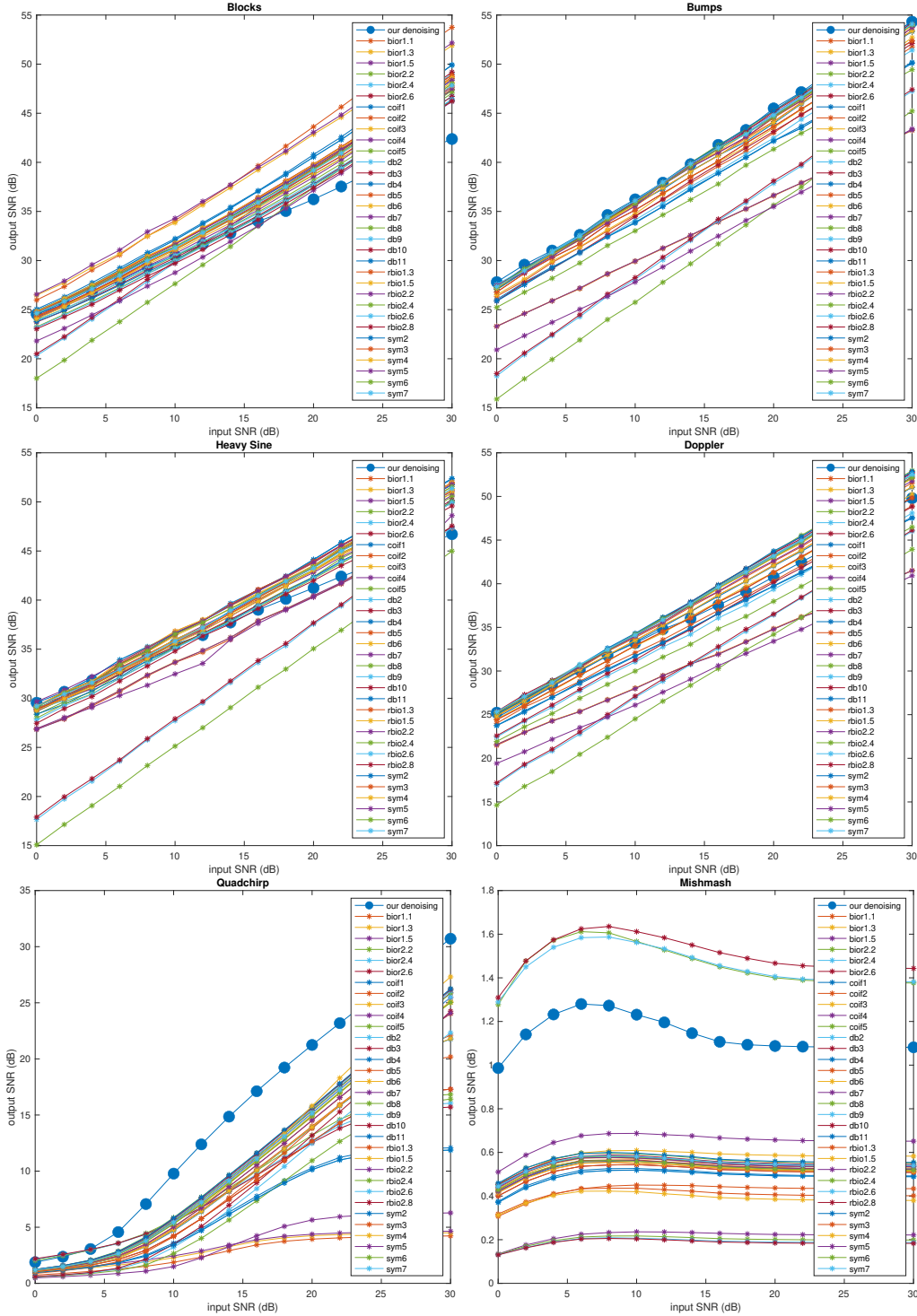


Figure 3: Comparison of our denoising method with the ones of “wdenoise” of Matlab for the six wavelet test functions: Blocks, Bumps, Heavy Sine, Doppler, Quadchirp, Mishmash.

other wavelets. Only 3 wavelets perform better: bior2.6, bior2.2 and bior2.4.

Overall, the performance of our basis varies depending on the signal type, never-

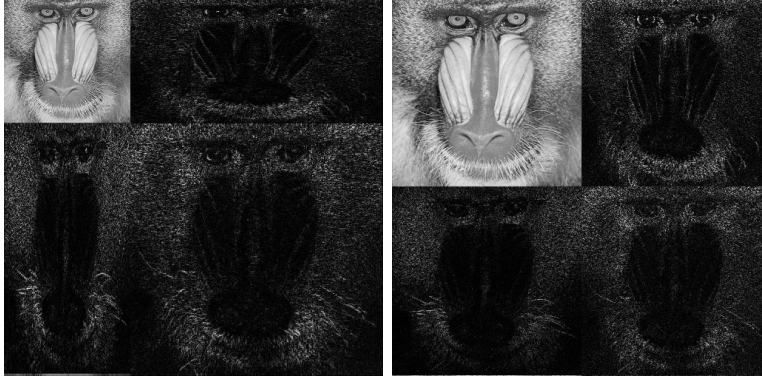


Figure 4: 1-level decomposition of the Baboon image with the tensor product VP wavelets (left) and the tensor product Daubechies wavelets (right)

theless the results highlight the robustness of our approach particularly in low-SNR conditions.

5. Image compression

Image compression is a key application of wavelet transforms, aimed at reducing storage and transmission costs while maintaining the perceptual quality of the data (see, e.g., [3, 4, 1, 2, 16, 9], among many others). In this section, we illustrate the performance of VP wavelets for image compression, comparing them with traditional separable wavelets. It is important to clarify that we use here the term "compression" somewhat loosely. Our approach involves only thresholding, without applying the full compression pipeline, which would typically include quantization and encoding. The goal of our study is in fact to assess the sparsifying ability - or compressibility - of the basis rather than to implement a complete compression scheme.

We present several tests, focusing on decomposition efficiency, the trade-offs in compression ratio (CR), defined as the ratio between the size of the original image and the size of the compressed image, and the impact of the parameter θ .

We first wish to illustrate the effect of a one-level decomposition using the VP basis. Fig. 4 presents the results of decomposing the classical Baboon image, comparing it to a standard wavelet tensor product decomposition (e.g., Daubechies 2). After just one level of decomposition, the approximation component retains only 1/3 of the original data size, with the remaining portion consisting of detail coefficients. This reduction means that fewer decomposition steps are required compared to the standard dyadic transform, for achieving a similar compact image representation, leading to significant computational savings.

To evaluate the quality of the VP basis for image compression, we conducted standard experiments involving the following steps: selecting a compression ratio (CR), or, equivalently, the percentage $P=100/CR$ of elements to be retained in the com-

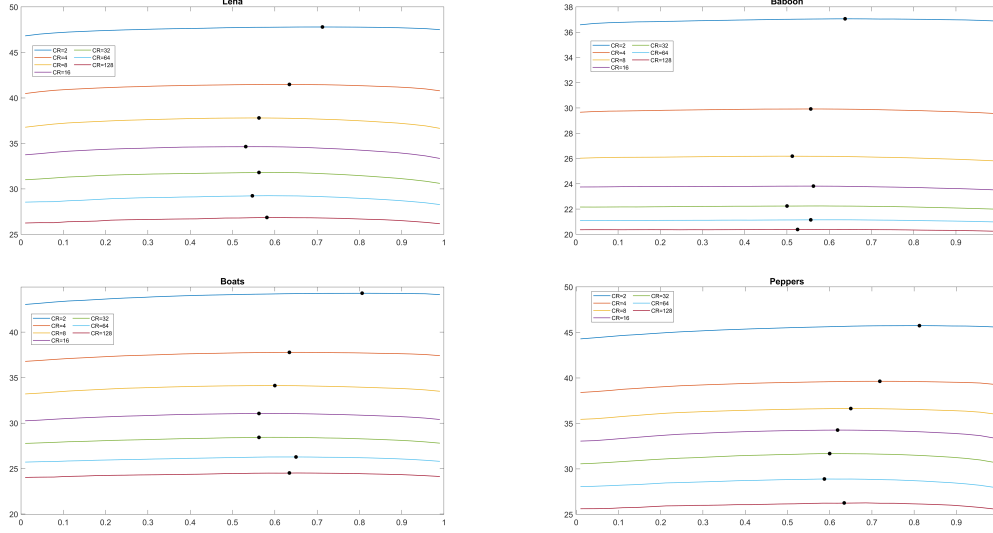


Figure 5: Variation of PSNR as a function of the free parameter θ for different images and compression ratios. The optimal θ for each curve is indicated by a black bullet.

pressed image; decomposing the image up to a certain level; zeroing wavelet coefficients below a threshold determined by the CR; and reconstructing the image.

The quality of the reconstruction is evaluated using both PSNR (Peak Signal-to-Noise Ratio) and SSIM (Structural Similarity Index Measure) metrics, and the results are compared to those achieved by using either the Daubechies filters with 4 coefficients (Db2) or the biorthogonal 3.5 (bior3.5) wavelets.

For standard wavelet decomposition and reconstruction, we used the MATLAB functions `wavedec2` and `waverec2`, respectively. The PSNR and SSIM quality metrics were computed using the MATLAB functions `psnr` and `ssim`.

The first tests were performed on four standard benchmark images: Lena, Baboon, Boats, and Peppers (each of size 512×512).

The dependency of the VP basis on the free parameter θ allows for its optimal selection in image reconstruction. To illustrate the effect of θ , Fig. 5 shows how the PSNR varies as a function of this parameter. This dependency is not uniform across all cases; rather, as observed, it is strongly influenced by the image data and the chosen compression ratio, which ranges as 2^k for $k = 1, \dots, 7$.

We now present a comparative analysis of the reconstruction quality between the VP basis and the biorthogonal spline wavelet filters bior3.5. We selected such filters because they are widely used in image compression, thanks to their symmetry, compact support, and high number of vanishing moments. The evaluation is performed in terms of PSNR and SSIM, considering their variation as a function of $\log_2(\text{CR})$. For this comparison, we have fixed seven levels of compression ratio, namely 2^k for $k = 1, \dots, 7$. For a fair comparison, since the images have all a size of 512×512 , we have considered 4 levels of decomposition for VP and 7 levels for the bior3.5

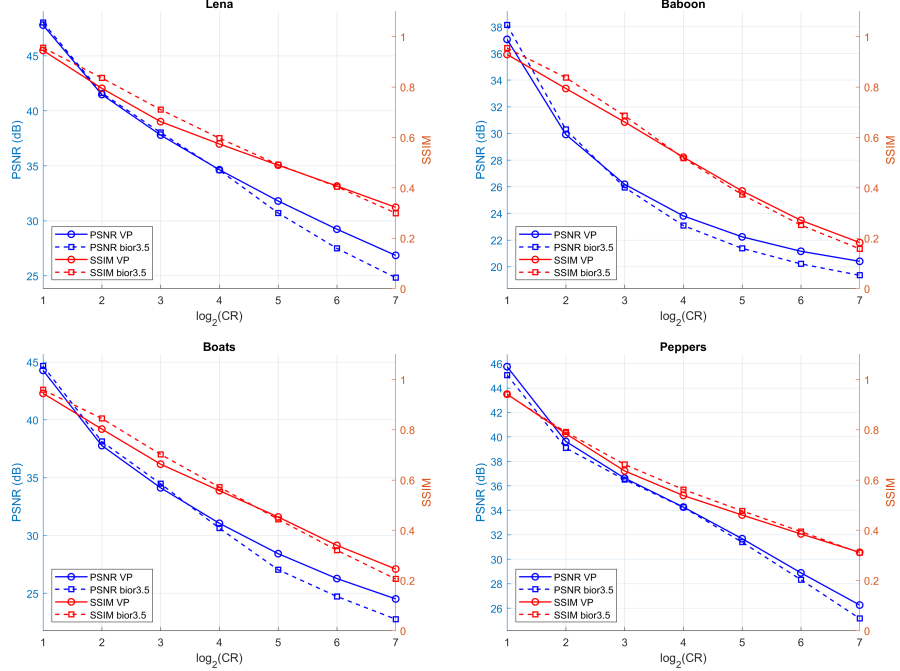


Figure 6: Comparison of reconstruction quality between VP and Bior3.5 wavelet filters in terms of PSNR and SSIM as a function of $\log_2(\text{CR})$ over different test images

filters, so that, at the very last level, a similar amount of approximation coefficients are retained (4 and 6, respectively). For the VP basis, a near-optimal θ parameter, providing nearly the best PSNR, was chosen from the interval $[0.5, 0.8]$ based on the experimental tests illustrated above.

From the plots in Fig. 6, it can be observed that the VP basis generally yields comparable or slightly higher PSNR and SSIM values than the bior3.5 wavelets across the given range of compression ratios for all four test images. In particular, for highly textured images (e.g., Baboon), the VP basis often maintains better performance at moderate to higher compression ratios, suggesting it can handle details effectively. For smoother images like Lena, its performance is still competitive and sometimes surpasses bior3.5.

We now present results for two larger images, "Airport" and "Man" shown in Fig. 7 on the left. Originally these images have size 1024×1024 , but we considered a cropped version of them, fixing the size to 729×729 . This (power of 3) size ensures compatibility with our algorithm without requiring additional adjustments to enforce a power-of-three size at each decomposition step, as described in Section 3.

The results shown on the two graphs on the right of Fig. 7 confirm that our basis outperforms bior3.5 for high-compression rates. While the performance appears similar or worse at lower compression rates, a closer visual inspection of the reconstructed images reveals that the VP basis produces quality, particularly in preserving fine

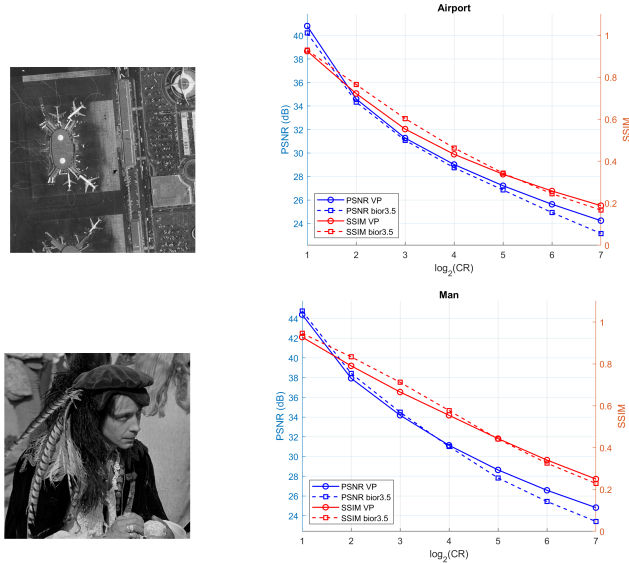


Figure 7: Comparison of reconstruction quality between VP and bior3.5 wavelet filters in terms of PSNR and SSIM as a function of $\log_2(\text{CR})$ over the two test images on the left image

details and reducing artifacts, as can be observed in Fig.8 for the Airport image.

As a further test, we compare the performance of VP wavelets with both the standard db2 and bior3.5 filters. For brevity, we show the results on three of the four 512×512 test images considered before, though several other images with different sizes have been considered in our experiments displaying similar behavior.

In order to highlight that our decomposition enables a reduction in computational cost while achieving similar or higher PSNR and SSIM values, Table 1 presents the results obtained after a single decomposition step for different percentages P of retained coefficients, i.e., keeping 50%, 40%, and 30% of the image data. We note that stronger compression cannot be considered with just one decomposition step, as there would not be enough wavelet coefficients to compress. In this regard, we point out that, for instance, $P = 25\%$ is allowed for VP wavelets but not for db2 and bior3.5.

Finally, without any limit on the decomposition steps, we considered different percentages $P = 100/\text{CR}$ of retained coefficients, including very large CR values. Table 2 displays the best results we obtained and the fewest decomposition steps required. As we can see, the performance of VP wavelets improves as P decreases (or CR increases), while for low CR values, db2 outperforms VP and bior3.5 wavelets, whose performances are almost comparable. In all cases, the decomposition steps required by VP wavelets are much fewer than those required by the other wavelets.

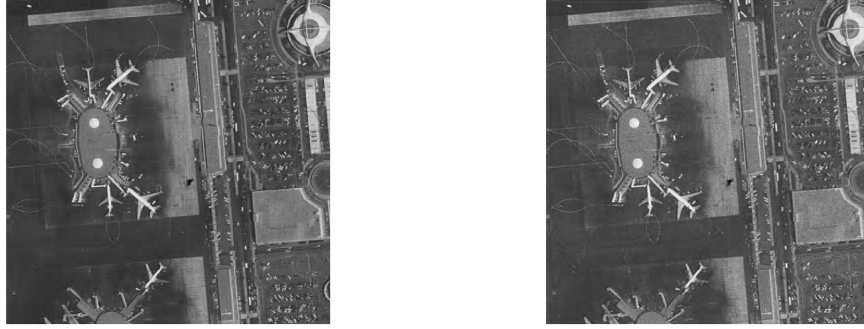


Figure 8: Reconstruction of the "Airport" image compressed at CR 1/16: VP (left) and bior3.5 (right).

Table 1: Compression performance after just 1 decomposition step

| | | Lena | | | Peppers | | | Baboon | | |
|-------|---------|--------|-------|-------|---------|-------|-------|--------|-------|-------|
| | | PSNR | SSIM | Steps | PSNR | SSIM | Steps | PSNR | SSIM | Steps |
| P=50% | VP | 47.354 | 0.940 | 1 | 45.293 | 0.936 | 1 | 36.581 | 0.924 | 1 |
| | db2 | 47.176 | 0.937 | 1 | 45.046 | 0.933 | 1 | 36.466 | 0.929 | 1 |
| | bior3.5 | 46.241 | 0.938 | 1 | 42.995 | 0.908 | 1 | 36.128 | 0.939 | 1 |
| P=40% | VP | 44.622 | 0.893 | 1 | 42.615 | 0.885 | 1 | 33.527 | 0.880 | 1 |
| | db2 | 43.859 | 0.878 | 1 | 41.888 | 0.870 | 1 | 33.648 | 0.887 | 1 |
| | bior3.5 | 43.859 | 0.878 | 1 | 40.464 | 0.846 | 1 | 32.687 | 0.899 | 1 |
| P=30% | VP | 42.049 | 0.821 | 1 | 40.151 | 0.809 | 1 | 30.510 | 0.827 | 1 |
| | db2 | 39.726 | 0.795 | 1 | 38.388 | 0.757 | 1 | 28.109 | 0.817 | 1 |
| | bior3.5 | 40.362 | 0.816 | 1 | 38.102 | 0.759 | 1 | 28.526 | 0.833 | 1 |

6. Conclusion

A new family of polynomial wavelets, based on de la Vallée Poussin interpolation and characterized by a free parameter, was recently introduced in [12], providing a solid theoretical foundation for future applications. In this study, after detailing the corresponding transform implementation, we evaluated the performance of these VP wavelets in two typical tasks — signal denoising and image compression — comparing them with classical wavelets.

The experimental results confirmed that VP wavelets offer competitive and satisfactory performance in both tasks, showing that VP wavelets are a viable alternative to standard wavelet approaches, providing robust reconstruction quality across different types of data.

In the experiments, the role of the free parameter θ was also observed experimentally.

For signal denoising, the value $\theta = 0.1$ was found to give better performance for the considered test signals. With this choice, the VP wavelet performs significantly better in the case of some test signals ("quadchirp" in particular), and for small input SNR, the VP wavelet gives results comparable to those of the standard wavelet

Table 2: Compression performance considering the best result achieved with the fewest decomposition steps

| | | Lena | | | Peppers | | | Baboon | | |
|--------|---------|--------|-------|-------|---------|-------|-------|--------|-------|-------|
| | | PSNR | SSIM | Steps | PSNR | SSIM | Steps | PSNR | SSIM | Steps |
| P=50% | VP | 47.797 | 0.945 | 3 | 45.743 | 0.942 | 3 | 37.056 | 0.930 | 3 |
| | db2 | 49.099 | 0.956 | 5 | 47.214 | 0.957 | 5 | 38.538 | 0.940 | 5 |
| | bior3.5 | 47.349 | 0.950 | 5 | 44.343 | 0.931 | 4 | 37.276 | 0.947 | 5 |
| P=25% | VP | 41.481 | 0.795 | 3 | 39.627 | 0.785 | 3 | 29.920 | 0.795 | 3 |
| | db2 | 42.218 | 0.805 | 6 | 40.640 | 0.815 | 5 | 30.877 | 0.801 | 6 |
| | bior3.5 | 41.415 | 0.830 | 5 | 38.928 | 0.784 | 5 | 30.009 | 0.830 | 6 |
| P=10% | VP | 36.730 | 0.632 | 3 | 35.860 | 0.600 | 3 | 25.323 | 0.619 | 3 |
| | db2 | 36.952 | 0.623 | 6 | 36.363 | 0.606 | 5 | 25.726 | 0.613 | 6 |
| | bior3.5 | 37.022 | 0.675 | 5 | 35.889 | 0.631 | 5 | 24.826 | 0.628 | 6 |
| P=5% | VP | 33.686 | 0.546 | 3 | 33.457 | 0.512 | 3 | 23.347 | 0.481 | 3 |
| | db2 | 33.516 | 0.526 | 6 | 33.726 | 0.511 | 8 | 23.460 | 0.470 | 7 |
| | bior3.5 | 33.838 | 0.578 | 6 | 33.650 | 0.539 | 5 | 22.453 | 0.465 | 6 |
| P=2% | VP | 30.138 | 0.440 | 3 | 29.901 | 0.412 | 3 | 21.502 | 0.309 | 4 |
| | db2 | 29.585 | 0.404 | 6 | 29.747 | 0.405 | 8 | 21.611 | 0.301 | 7 |
| | bior3.5 | 29.900 | 0.455 | 7 | 29.698 | 0.433 | 6 | 20.700 | 0.294 | 6 |
| P=1% | VP | 27.686 | 0.352 | 3 | 27.170 | 0.338 | 3 | 20.654 | 0.212 | 4 |
| | db2 | 27.035 | 0.319 | 8 | 26.924 | 0.330 | 8 | 20.702 | 0.201 | 7 |
| | bior3.5 | 27.002 | 0.359 | 6 | 26.667 | 0.351 | 6 | 19.880 | 0.198 | 7 |
| P=0.5% | VP | 25.443 | 0.275 | 4 | 24.666 | 0.267 | 3 | 20.041 | 0.144 | 4 |
| | db2 | 24.864 | 0.242 | 8 | 24.527 | 0.256 | 8 | 20.035 | 0.131 | 9 |
| | bior3.5 | 24.590 | 0.273 | 7 | 24.259 | 0.277 | 9 | 19.378 | 0.129 | 7 |

approaches.

In image compression, we observed that the value of θ providing the best performance is strongly influenced by the image data and the fixed compression ratio. For the “best” parameter choice, all the experiments revealed much better performance for larger compression ratios (i.e., smaller percentages of retained data) in comparison with Daubechies and biorthogonal wavelets.

Nevertheless, with only one decomposition step, VP wavelets always outperform both Daubechies and biorthogonal wavelets. Indeed, compared to classical wavelets, VP wavelets have the advantage of considering multiples of 3 instead of 2 in the downsampling step of a multiresolution analysis.

As a further advantage, they do not require periodization or zero-padding techniques because they are defined on a compact interval.

A disadvantage is their non-orthogonality, which led us to introduce appropriate normalization factors for energy preservation. These factors have been determined theoretically, starting from the Riesz stability properties in (8) and (9), which establish an equivalence between continuous and discrete norms. In such equivalences, the involved constants are independent of the data and the resolution level but depend on the θ parameter. For denoising, these normalization factors have been further refined, with experimental values obtained.

In future research, we aim to find better values for the normalization factors. We have observed that these factors are dependent on the choice of θ , which deserves further investigation.

We also aim to explore other applications that can best exploit the regularity, interpolation, and uniform near-best approximation properties offered by VP wavelets.

Acknowledgments

The first two authors are members of RITA (Research Italian Network on Approximation), of UMI-TAA research group, and Gruppo Nazionale Calcolo Scientifico-Istituto Nazionale di Alta Matematica (GNCS-INdAM) which partially supported this work. The first author was also partially supported by the EU under the Italian National Recovery and Resilience Plan (PNRR) of NextGenerationEU, partnership on “Telecommunications of the Future” (PE000000001 - program “RESTART”). The research of the third author was partially supported by the Fund for Scientific Research – Flanders (Belgium), project G0B0123N.

References

- [1] V. Alarcón-Aquino, J. M. Ramírez-Cortés, P. Gómez-Gil, O. Starostenko, H. Lobato-Morales, Lossy image compression using discrete wavelet transform and thresholding techniques, *The Open Cybernetics & Systemics Journal* 7 (2013) 32–38.
- [2] M. Boix, B. Cantó, Wavelet transform application to the compression of images, *Mathematical and Computer Modelling* 52 (7) (2010) 1265–1270.
- [3] V. Bruni, M. Cotronei, F. Pitolli, A family of level-dependent biorthogonal wavelet filters for image processing, *Journal of Computational and Applied Mathematics* 367 (2020) 112467.
- [4] S. Chang, B. Yu, M. Vetterli, Adaptive wavelet thresholding for image denoising and compression, *IEEE Transactions on Image Processing* 9 (9) (2000) 1532–1546.
- [5] H. A. Chipman, E. D. Kolaczyk, R. E. McCulloch, Adaptive bayesian wavelet shrinkage, *Journal of the American Statistical Association* 92 (440) (1997) 1413–1421.
- [6] D. L. Donoho, I. M. Johnstone, Ideal spatial adaptation by wavelet shrinkage, *Biometrika* 81 (3) (1994) 425–455.
- [7] D. L. Donoho, De-noising by soft-thresholding, *IEEE Transactions on Information Theory* 41 (3) (1995) 613–627.
- [8] Z. Ditzian, V. Totik, *Moduli of smoothness*, Springer-Verlag, New York, 1987.
- [9] H. Ma, D. Liu, N. Yan, H. Li, F. Wu, End-to-end optimized versatile image compression with wavelet-like transform, *IEEE Transactions on Pattern Analysis and Machine Intelligence* 44 (3) (2022) 1247–1263.

- [10] D. Occorsio, W. Themistoclakis, On the filtered polynomial interpolation at Chebyshev nodes, *Appl. Numer. Math.* 166 (2021) 272–287.
- [11] D. Occorsio, W. Themistoclakis, Some remarks on filtered polynomial interpolation at Chebyshev nodes, *Dolomites Research Notes on Approximation* 14 (2) (2021) 68–84.
- [12] W. Themistoclakis, M. Van Barel, A free parameter depending family of polynomial wavelets on a compact interval, submitted.
- [13] W. Themistoclakis, Some interpolating operators of de la Vallée Poussin type, *Acta Mathematica Hungarica* 84 (3) (1999) 221 – 235.
- [14] W. Themistoclakis, Uniform approximation on $[-1, 1]$ via discrete de la Vallée Poussin means, *Numerical Algorithms* 60 (4) (2012) 593 – 612.
- [15] W. Themistoclakis, Weighted L^1 approximation on $[-1,1]$ via discrete de la Vallée Poussin means, *Mathematics and Computers in Simulation* 147 (2018) 279 – 292.
- [16] B. Usevitch, A tutorial on modern lossy wavelet image compression: foundations of jpeg 2000, *IEEE Signal Processing Magazine* 18 (5) (2001) 22–35.